

LETTER TO THE EDITOR

Spectroscopy of the Supernova H0pe Host Galaxy at Redshift 1.78

M. Polletta¹, M. Nonino², B. Frye³, A. Gargiulo¹, S. Bisogni¹, N. Garuda³, D. Thompson⁴, M. Lehnert⁵, M. Pascale⁶, S. P. Willner⁷, P. Kamieneski⁸, R. Leimbach³, C. Cheng^{9,10}, D. Coe^{11,12,13}, S. H. Cohen⁸, C. J. Conselice¹⁴, L. Dai¹⁵, J. Diego¹⁶, H. Dole¹⁷, S. P. Driver¹⁸, J. C. J. D'Silva^{18,19}, A. Fontana²⁰, N. Foo³, L. J. Furtak²¹, N. A. Grogin¹¹, K. Harrington²², N. P. Hathi¹¹, R. A. Jansen⁸, P. Kelly²³, A. M. Koekemoer¹¹, C. Mancini¹, M. A. Marshall^{24,19}, J. D. R. Pierel¹¹, N. Pirzkal¹¹, A. Robotham¹⁸, M. J. Rutkowski²⁵, R. E. Ryan, Jr.¹¹, J. M. Snigula²⁶, J. Summers⁸, S. Tompkins⁸, C. N. A. Willmer³, R. A. Windhorst⁸, H. Yan²⁷, M. S. Yun²⁸, and A. Zitrin²¹

(Affiliations can be found after the references)

Received 22 May 2023 / Accepted 20 June 2023

ABSTRACT

Supernova (SN) H0pe was discovered as a new transient in James Webb Space Telescope (*JWST*) NIRCam images of the galaxy cluster PLCK G165.7+67.0 taken as part of the “Prime Extragalactic Areas for Reionization and Lensing Science” (PEARLS) *JWST* GTO program (# 1176) on 2023 March 30 (AstroNote 2023-96; Frye et al. 2023). The transient is a compact source associated with a background galaxy that is stretched and triply-imaged by the cluster’s strong gravitational lensing. This paper reports spectra in the 950–1370 nm observer frame of two of the galaxy’s images obtained with Large Binocular Telescope (LBT) Utility Camera in the Infrared (LUCI) in longslit mode two weeks after the *JWST* observations. The individual and average spectra show the [O II] $\lambda\lambda 3727, 3730$ doublet and the Balmer and 4000 Å breaks at redshift $z=1.783\pm 0.002$. The Code Investigating GALaxy Emission (CIGALE) best-fit model of the spectral energy distribution indicates that SN H0pe’s host galaxy is massive ($M_{\text{star}}\approx 6\times 10^{10} M_{\odot}$ after correcting for a magnification factor $\mu\sim 7$) with a predominant intermediate age (~ 2 Gyr) stellar population, moderate extinction, and a magnification-corrected star formation rate $\approx 13 M_{\odot} \text{ yr}^{-1}$, consistent with being below the main sequence of star formation. These properties suggest that H0pe might be a type Ia SN. Additional observations of SN H0pe and its host recently carried out with *JWST* (*JWST*-DD-4446; PI: B. Frye) will be able to both determine the SN classification and confirm its association with the galaxy analyzed in this work.

Key words. Galaxies: high-redshift, Galaxies: star formation, Stars:supernovae: individual: SN H0pe

1. Introduction

The James Webb Space Telescope (*JWST*; Gardner et al. 2006; Rieke et al. 2005; Beichman et al. 2012; Windhorst et al. 2008), with its unprecedented sensitivity and spatial resolution at infrared wavelengths, can be used as a time machine to capture the light even from single stars early in the history of the Universe from their birth in a dusty cradle to their spectacular death in the form of supernovae (SNe) (Welch et al. 2022; Diego et al. 2023; Vanzella et al. 2023; Meena et al. 2023; Kelly et al. 2023).

Recently, Frye et al. (2023) announced the discovery of a SN in a galaxy at a photometric redshift of ~ 1.8 in *JWST*/NIRCam multi-band observations obtained as part of the “Prime Extragalactic Areas for Reionization and Lensing Science” (“PEARLS”) GTO Program (# 1176, PI: Windhorst; Windhorst et al. 2023) in the PLCK G165.7+67.0 (G165 hereinafter) field. G165 is a massive ($M_{600\text{kpc}} = 2.4 \times 10^{14} M_{\odot}$) galaxy cluster at $z=0.35$ (Cañameras et al. 2018; Frye et al. 2019; Pascale et al. 2022). The cluster strongly lenses numerous background galaxies including bright sub-millimeter (sub-mm) galaxies at $z\gtrsim 2$ (Harrington et al. 2016), and indeed G165 was discovered by the *Planck* telescope because of its bright sub-mm emission (Planck Collaboration et al. 2015, 2016). Comparison of the new *JWST*/NIRCam images with psf-matched archival images from Wide Field Camera 3 (WFC3) on the *Hubble Space Telescope* (*HST*; Miley et al. 2004; Zirm et al. 2005) revealed

a new, pointlike source associated with a triply-imaged galaxy. The magnification factor of the lensed galaxy is estimated to be $\mu\sim 3-16$ across the three images, designated as 2a, 2b, and 2c (Fig. 1; Frye et al. 2019; Pascale et al. 2022, Kamieneski, priv. comm.). The new source, visible next to all three of the lensed galaxy images (see Fig. 2), was named “SN H0pe” because it offers the potential of a new, independent measurement of the Hubble–Lemaître constant H_0 .

The apparent SN discovery prompted follow-up spectroscopic observations with the goal of measuring the spectroscopic redshift of the host galaxy. The redshift was needed to plan effective observations to determine the redshift and type of the SN. Because the SN light fades with time, these observations had to be carried out as soon as possible after the SN’s discovery. Through a concerted effort of the Large Binocular Telescope (LBT; Hill et al. 2012) consortium, longslit spectroscopic observations with the LBT Utility Camera in the Infrared (LUCI; Seifert et al. 2003, 2010; Ageorges et al. 2010; Buschkamp et al. 2012) were quickly planned, carried out, reduced, and analyzed.

This Letter presents the results of the LUCI observations: the first spectroscopic measurement and characterization of the SN H0pe host galaxy. The study of even a single SN host galaxy is important to learn about SN progenitors, SN host demographics, and to quantify age, metallicity, and dust extinction effects on SN measurements. This is especially relevant at high redshift as some evolutionary trends could mimic cosmological effects.

Additional spectroscopic and multi-epoch imaging observations were carried out with *JWST* after the LBT observa-

Send offprint requests to: M. Polletta
e-mail: maria.polletta@inaf.it

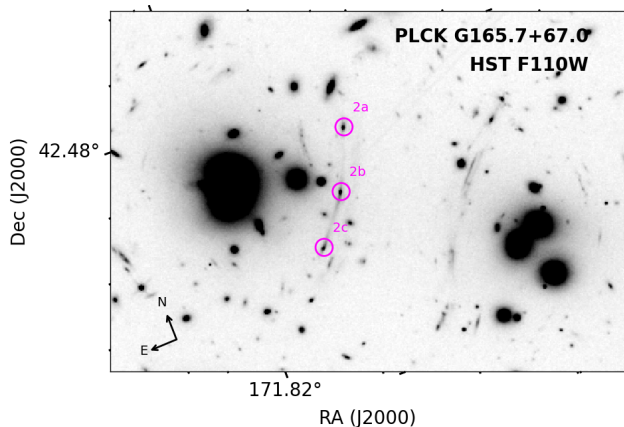


Fig. 1. Archival *HST*/WFC3 F110W negative image of the PLCK G165.7+67.0 field ($1' \times 0.7'$). The triply-imaged arcs 2a, 2b, and 2c of the SN H0pe host galaxy are highlighted with $1''$ -radius magenta circles (credits: Frye et al. 2019). The highlighted regions are part of an arc produced by strong lensing from the foreground galaxy cluster.

tions (Program *JWST*-DD-4446; PI: B. Frye). These observations, which will be presented in a future work, will help to establish the SN type, verify its association with the triply-imaged galaxy, and measure H_0 . Throughout this study, we adopt a Chabrier (2003) initial mass function (IMF) and a flat Λ cold dark matter (CDM) model with cosmological parameters from the Planck 2018 release (i.e., $\Omega_\Lambda = 0.685$; $\Omega_m = 0.315$; $H_0 = 67.4 \text{ km s}^{-1} \text{ Mpc}^{-1}$; Planck Collaboration et al. 2020). All colors and magnitudes quoted in this paper are expressed in the AB system (Oke & Gunn 1983).

2. Large Binocular Telescope spectroscopic observations

Longslit spectroscopic observations of the SN host were obtained with LUCI on the LBT (Program INAF-2023A-777; PI: M. Nonino). Observations were carried out on UT 2023 April 16 by the LBTB team with the support of the University of Arizona LBT staff. Observations used the N1.8 camera ($0''.249/\text{pixel}$) and the second order of the G200 grating with the zSpec filter resulting in wavelength coverage from 950 to 1370 nm in the observer frame. The slit width was $1''$, which results in a spectral resolution $R \sim 1200$, sufficient to identify the 400 nm break, strong emission lines, and absorption features at the expected source redshift. The main goal of these observations was to obtain a spectroscopic redshift and the optical rest-frame spectrum of two images of the galaxy associated with SN H0pe, sources 2a ($\alpha_{2000} = 11:27:15.33$; $\delta_{2000} = 42:28:41.07$), and 2b ($\alpha_{2000} = 11:27:15.60$; $\delta_{2000} = 42:28:34.13$) (Frye et al. 2019). To center the $1'' \times 200''$ longslit on source 2b, the brighter of the two target images, the telescope was blindly offset by $\sim 5''$ from a bright source. The slit had a position angle (PA) of 157° in order to include also image 2a of the SN host. Fig. 2 shows a multi-band *JWST* image from the PEARLS Program of the two host images with the longslit position superimposed. The respective SN images were also in the slit but probably contributed $< 8\%$ of the observed light ($m(\text{F160W})_{2b} \approx 21.12$ versus $m(\text{F150W})_{\text{SNb}} \approx 23.91$; Pascale et al. 2022; Frye et al. 2023.) Eight additional objects, of which six are within the *JWST*/NIRCam field-of-view, were serendipitously detected in the slit. These other objects will be discussed in a future work.

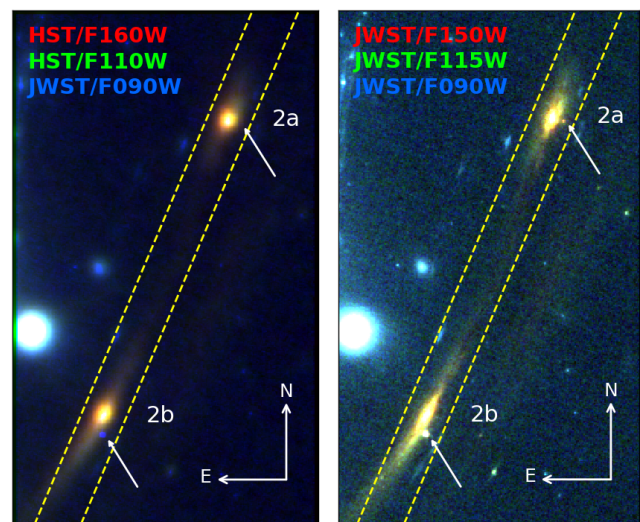


Fig. 2. Multi-band $7'' \times 12''$ images of SN HOPE and its host galaxy. *Left panel:* HST images taken in 2015–2016 (red: HST/F160W, green: HST/F110W, Cy23, GO-14223, PI: Frye) and *JWST* image (blue: F090W) taken on 2023 March 30, about two weeks before the LBT spectroscopic observation reported here. *Right panel:* *JWST* images taken on 2023 March 30 (red: *JWST*/F150W, green: *JWST*/F115W, and blue: *JWST*/F090W). *JWST* images are from the PEARLS GTO program and are adapted from <https://www.as.arizona.edu/bright-and-shiny-result-pearls>. The two SN H0pe host-galaxy images 2a and 2b are labeled, and the SN positions are marked with white arrows. Dashed yellow lines mark the slit edges at $\text{PA} = 157^\circ$.

The observations were carried out in binocular mode and divided into 36 300 s exposures per arm, resulting into a total exposure time of 6 hours. The telescope was “nodded” along the direction of the slit with $4''$ offsets to obtain good sky subtraction during the data reduction. A star was observed at the end of the observations for flux calibration and to correct for atmospheric absorption. Flat-field exposures were taken on the same day as the observations. The observing conditions were good with a clear sky, an average airmass of 1.03, and seeing $1''$.

Data reduction was carried out by the Italian LBT support team using the Spectroscopic Interactive Pipeline and Graphical Interface (SIPGI) pipeline developed at INAF IASF-Milan (Gargiulo et al. 2022). This included flat-fielding, dark subtraction, sky subtraction, correction for bad pixels, cosmic rays, and distortions, and wavelength and flux calibration. From each scientific exposure, the background level was first removed by subtracting the subsequent dithered frame in the observing sequence. Possible background residuals were then estimated and removed by fitting all the pixels on the sky along the spatial direction of each column with a polynomial. Wavelength calibration was carried out using OH sky lines and reaches an accuracy of 0.25 \AA . For each source detected in the final flux-calibrated 2-d spectrum, the flux calibrated 1-d spectrum was extracted, and the associated sky and noise spectra were produced.

3. Spectroscopic redshift measurement

The LBT spectra of 2a and 2b are shown in Fig. 3 along with their average, and the sky spectrum. We measured the redshift of each spectrum and of the averaged one using the EZ code (Gargiulo et al. 2010). EZ derives the redshift through a weighted cross-correlation between the observed spectrum over a specific wavelength range (980–1350 nm in this case) and a library of galaxy

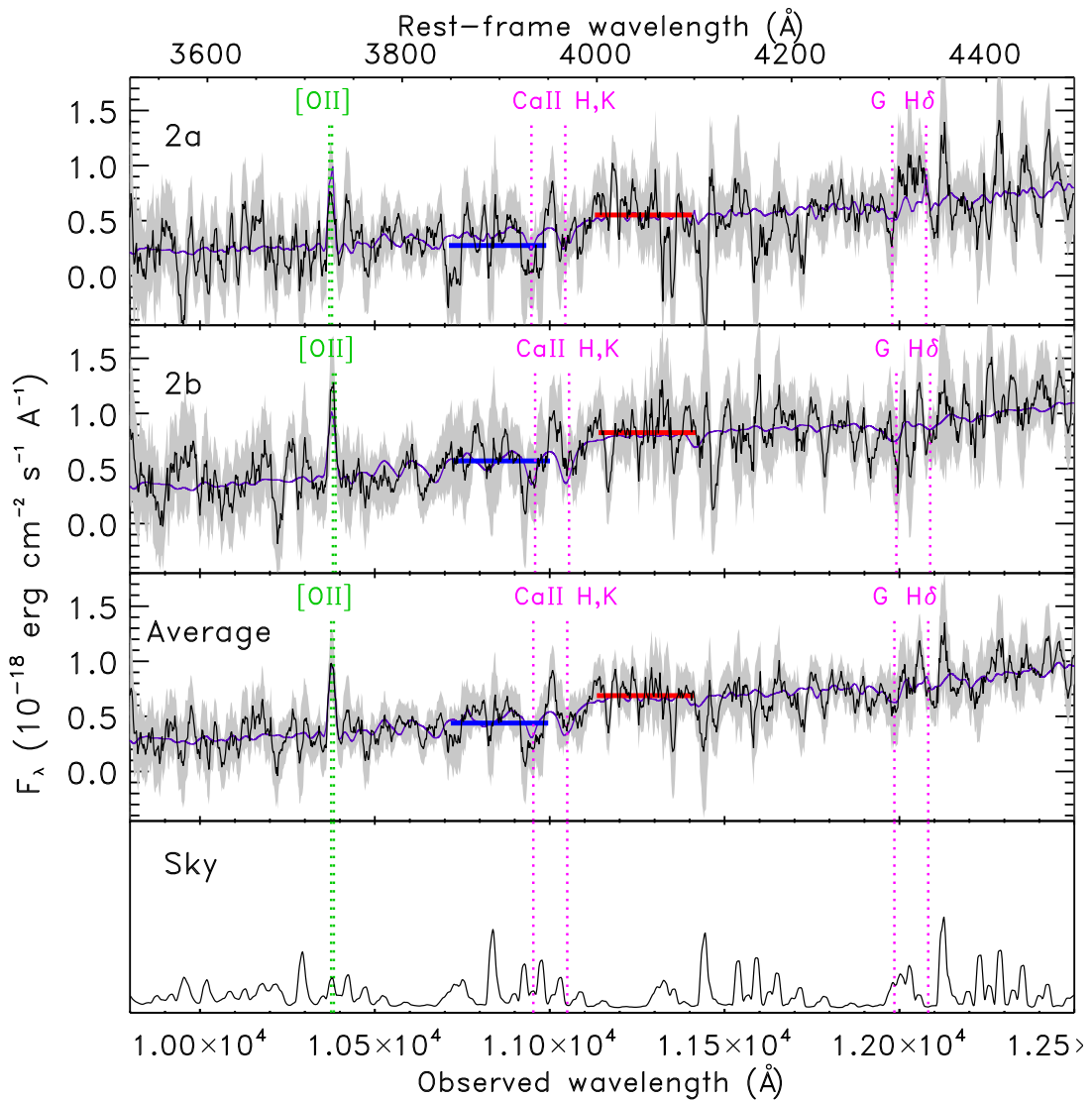


Fig. 3. Smoothed ($\Delta\lambda=17.2\text{ \AA}$) and cropped LBT/LUCI spectra (black solid line) of the SN H0pe host from image 2a (*top panel*), 2b (*second panel*), the averaged spectrum (*third panel*), and the sky (*bottom panel*). The grey shaded area shows the 1σ noise. The main spectral features are labeled with green (for emission) and magenta (for absorption) vertical dotted lines. The purple line represents the Bagpipes best-fit model. The average flux densities in the rest-frame wavelength intervals 385–394 nm and 400–410 nm, used to compute the $D4000_n$ index, are shown with blue and red horizontal lines, respectively.

spectral templates. EZ takes into account the presence of strong emission features as well as of the continuum shape in the redshift determination. EZ selected as best-fit template a red elliptical at $\langle z_{\text{spec}} \rangle = 1.783$ ($z = 1.782, 1.784, \text{ and } 1.783$ for 2a, 2b, and the averaged spectrum, respectively). Because EZ uses a library of templates rather than actual fits, we derived the best spectral model using the Bagpipes code (Carnall et al. 2021). The redshifts were fixed at the measured values, and other parameters included a double-exponential star-formation history (SFH), the stellar population models of Bruzual & Charlot (2003), and the Calzetti et al. (2000) attenuation law. The Bagpipes best fit-models at the EZ spectroscopic redshifts, shown in Fig. 3, are consistent with the spectra having Ca II HK K and H absorption lines (at rest 3934.8 Å and 3969.6 Å), the [O II] $\lambda\lambda 3727, 3730$ doublet, and the Balmer (3646 Å) and 4000 Å breaks. The signal-to-noise ratios (SNRs) of the [O II], K and H lines, computed as the difference between the line peak and the interpolated continuum at the line wavelength divided by the rms of the spectrum in

a 200 Å region centered on each line, are, respectively, 3.5, 0.6, and 0.7. The measured Balmer and 4000 Å breaks¹ are, respectively, 1.48 ± 0.25 and 1.57 ± 0.25 . While the only spectral features significantly detected individually are the [O II] doublet and the breaks in the continuum, all features contribute to the correlation signal. The width of [O II] doublet constrains the spectroscopic redshift to be between 1.781 and 1.785, consistent with the EZ measurement, and we therefore report $z = 1.783 \pm 0.002$ as a best estimate and conservative uncertainty. This spectroscopic redshift is an important factor for obtaining a robust lens model of the triply-imaged system and enabling precision cosmology with SN H0pe (Johnson & Sharon 2016).

¹ The 4000 Å break is quantified through the $D4000_n$ index (Balogh et al. 1999). This was computed as the ratio between the average flux density in the wavelength intervals 400–410 nm and 385–395 nm. The Balmer break was computed as the ratio between the average flux density in the wavelength intervals 380–395 nm and 350–365 nm.

4. Properties of the SN host galaxy

To characterize the SN host, we analyzed its spectral energy distribution (SED). For this study, we consider only source 2b, for which multi-band photometric measurements are available (see ID 3 in Table 2 of Pascale et al. 2022). The data include LBT/LBC (g and i), *HST*/WFC3 (F110W, F160W), LBT/LUCI (K), and *Spitzer*/IRAC (3.6, 4.5 μm). Based on a preliminary analysis of the *JWST*/NIRCam imaging, these measurements are affected by a magnification factor $\mu \approx 7.4^{+8.9}_{-3.7}$ (P. Kamienski, priv. comm.). We modeled the SED of source 2b with the Code In-

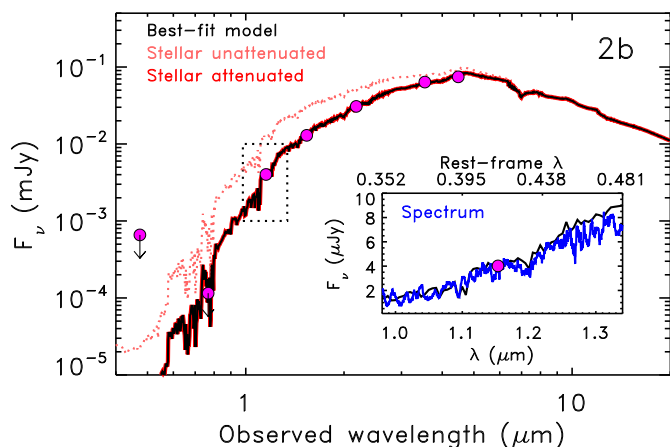


Fig. 4. Spectral energy distributions of the SN H0pe host image 2b. Magenta filled circles show the observed photometry, not corrected for magnification, and arrows represent 5σ upper limits. The CIGALE best-fit model is shown with a black solid line, the light red dotted line shows the stellar light before dust attenuation, and the red solid line (coincident with the black line) shows the attenuated stellar light. The inset shows the smoothed LBT 1-d spectra (blue solid line), the best-fit SED (black line), and the F110W photometric data point (magenta filled circle) in the ranges shown by the dotted rectangles in the main panel.

vestigating Galaxy Emission (CIGALE; Boquien et al. 2019). The code provides constraints on the age of the stellar components and estimates of dust extinction, stellar mass, and SFR. We fixed the redshift at the EZ value obtained from the spectrum and adopted a model with a delayed star formation history (SFH), a Chabrier (2003) initial mass function (IMF), the stellar population models of Bruzual & Charlot (2003), solar metallicity ($Z = 0.02$), and the Calzetti et al. (2000) attenuation law. The best fit was determined as the template with the lowest χ^2 , and the best-fit parameters and associated uncertainties are the likelihood-weighted means and standard deviations, respectively. The results are consistent with the spectral fit from Bagpipes. The derived stellar age is 2.5 ± 0.5 Gyr, and the magnified stellar mass and SFR (i.e., as calculated without correcting for magnification) are, respectively, $\log(\mu M_{\text{star}}/M_{\odot}) = 11.6 \pm 0.1$ and $\mu\text{SFR} < 130 M_{\odot} \text{yr}^{-1}$, the latter only an upper limit. The fit requires a significant amount of dust extinction, $A_V = 1.2 \pm 0.4$. Fig. 4 shows the model, the photometry, and the LBT flux-calibrated 1-d spectra. There is good agreement between the 1-d spectrum and the SED, demonstrating the goodness of the spectral flux calibration. In summary, the CIGALE model indicates that the SN host is a dust-obscured massive galaxy of intermediate age.

An independent measurement of the galaxy SFR can be obtained from the luminosity of the [O II] doublet, which is pro-

duced by ionized gas in star-forming regions. (Neither the spectrum nor the photometry show any evidence of an active galactic nucleus, and no pointlike nucleus is seen in the *HST* images.) The [O II] flux obtained by fitting the doublet with a Gaussian profile in the average spectrum is $(1.4 \pm 0.2) \times 10^{-17} \text{ ergs cm}^{-2} \text{ s}^{-1}$. The SFR–L([O II]) relation depends on oxygen abundance (eq. 5 of Zhuang & Ho 2019). For the SN host galaxy, we adopted $\log(\text{O}/\text{H}) + 12 = 9.02$, the value typical of massive galaxies as the CIGALE fit shows the SN host to be.² This gives magnified $\mu\text{SFR} = (2.5 \pm 0.4) M_{\odot} \text{yr}^{-1}$ for the average spectrum. If the [O II] lines suffer extinction 3.95 mag,³ and the magnification factor $\mu \approx 7$ (Kamienski, priv. comm.), the magnification- and dust-corrected SFR $\approx (13 \pm 2) M_{\odot} \text{yr}^{-1}$. The true SFR might be smaller if diffuse stellar sources such as hot post-asymptotic giant branch stars contribute to [O II] (e.g., Belfiore et al. 2016).

The main-sequence SFR for a galaxy of the same mass (corrected for $\mu \approx 7$) and redshift is $82^{+48}_{-31} M_{\odot} \text{yr}^{-1}$, where the uncertainty is derived from the 0.2 dex scatter (Speagle et al. 2014). The [O II] SFR is therefore below the main sequence value, implying that this system might be transitioning to or already in a passive phase. The galaxy spectrum (Fig. 3) exhibits a 4000 Å break, which is developed by a passively evolving stellar population at 500 Myr (Bica et al. 1994) and strengthens with age (Kauffmann et al. 2003). The $D4000_n$ value in the average spectrum is 1.6 ± 0.3 , consistent with the value $D4000_n \approx 1.55$ usually adopted to separate star-forming and passive galaxies (e.g., Gargiulo et al. 2017; Haines et al. 2017). Thus $D4000_n$ agrees with the CIGALE age and with this system being on its way to becoming a passive galaxy.

5. Discussion and perspectives

Discovery of distant SNe and study of their hosts are important for precision cosmology because the SN properties (i.e., luminosity at maximum and rate of decline) depend on host properties (Hamuy et al. 1995; Sullivan et al. 2006; Williams et al. 2020), and any systematic trends of the latter with redshift could mimic a cosmological effect (Williams et al. 2003; Sullivan et al. 2003; Combes 2004). Examples include redshift-dependent reddening laws (Totani & Kobayashi 1999) or element abundance ratios of the progenitor stars (Höflich et al. 2000; Drell et al. 2000). If the association of SN H0pe with the triply-imaged galaxies 2a, 2b, and 2c is confirmed, this SN would be among the most distant known SNe. Indeed, to our knowledge and without considering the super luminous SNe (Khetan et al. 2023), today there are only four known SNe at $z \geq 1.8$ (i.e., $1.80 < z < 2.26$; Jones et al. 2013; Rodney et al. 2015; Rubin et al. 2018), and SN H0pe is the only one with *JWST* data. This system thus offers an excellent opportunity to study in detail a high- z SN host, and the SN itself.

The SN H0pe host-galaxy SED indicate that this system, after correcting for a magnification factor $\mu = 7$, is a massive ($M_{\text{star}} \sim (6.0 \pm 0.8) \times 10^{10} M_{\odot}$) galaxy of intermediate age (2.5 ± 0.5 Gyr) with significant extinction and low star-formation rate (SFR $\approx (13 \pm 2) M_{\odot} \text{yr}^{-1}$), implying that it might be on its way to becoming or be quiescent (Speagle et al. 2014). This finding suggests that H0pe might be a type Ia SN, as these occur in all type of galaxies, whereas core-collapse SNe are only found

² For this abundance, $\text{SFR}/(M_{\odot} \text{yr}^{-1}) = 7.74 \times 10^{-42} L_{[\text{O II}]} / (\text{erg s}^{-1})$ (Zhuang & Ho 2019).

³ The Calzetti et al. (2000) reddening curve gives $A_{3728\text{\AA}} = 1.45 \times A_V$, but in addition, star-forming gas clouds have higher extinction than the stellar population (Calzetti 1997), $E_{\text{gas}}(B-V) = E_{\text{star}}(B-V) / (0.44 \pm 0.03)$.

in star forming galaxies (Kelly & Kirshner 2012). Since only one third of SNe Ia is found in early-type systems, locally and up to intermediate redshifts (Farrah et al. 2002), it is quite exceptional to have caught this SN in such a galaxy. Furthermore, SNe are more difficult to observe in galaxies that suffer from dust obscuration. Again, SN Hope beats the odds because of the significant extinction derived for its host. The host red color and extinction are unusual among both main-sequence star-forming galaxies (Pacifci et al. 2023) and quiescent galaxies (D'Eugenio et al. 2021). A possible explanation is that the obscuring dust might be in the foreground, perhaps associated with the G165 cluster as previously suggested by Pascale et al. (2022), but this hypothesis seems unlikely as there is no sign of an intervening galaxy. Intergalactic dust is also implausible because it would not cause reddening (Aguirre & Haiman 2000). The amount of dust extinction, the level of star-formation activity, and the lensing magnification factor in this galaxy are quite uncertain, and more study is needed to pin down the values. However, the overall characterization of the galaxy as massive and nearing or at quiescence should be secure. Aside from its intrinsic interest, characterizing the dust properties of the SN H0pe host is necessary to correctly analyze the SN measurements.

Analysis of the *JWST* data from the PEARLS program and the more recent DD observations will yield an improved SED measurement of the triply-imaged host and a refined lens model. These will provide better constraints on the system star-formation activity level and stellar age. In addition, it will be possible to investigate whether the SN suffers dust extinction and how this might affect the SN measurements. The *JWST* data will also determine the SN classification, test its association with the triply-imaged galaxy, measure time delays of the three lensed images, and provide a precise measurement of H_0 (see e.g., Kelly et al. 2023).

Acknowledgements. We kindly thank the referee for promptly reviewing the manuscript. M.P. kindly thanks M. Fumana, and P. Franzetti for their assistance in installing and using EZ, F. Cusano for his prompt help with the LBT data retrieval, and D. Burgarella for his support with CIGALE. B.L.F. obtained student support through a Faculty Challenge Grant for Increasing Access to Undergraduate Research, and the Arthur L. and Lee G. Herbst Endowment for Innovation and the Science Dean's Innovation and Education Fund, both obtained at the University of Arizona. AZ and L.J.F. acknowledge support by Grant No. 2020750 from the United States-Israel Binational Science Foundation (BSF) and Grant No. 2109066 from the United States National Science Foundation (NSF), and by the Ministry of Science & Technology, Israel. The LBT is an international collaboration among institutions in the United States, Italy and Germany. LBT Corporation partners are: The University of Arizona on behalf of the Arizona university system; Istituto Nazionale di Astrofisica, Italy; LBT Beteiligungsgesellschaft, Germany, representing the Max-Planck Society, the Astrophysical Institute Potsdam, and Heidelberg University; The Ohio State University, and The Research Corporation, on behalf of The University of Notre Dame, University of Minnesota, and University of Virginia. We acknowledge the support from the LBT-Italian Coordination Facility for the execution of observations, data distribution and reduction. This research is based on observations made with the NASA/ESA Hubble Space Telescope obtained from the Space Telescope Science Institute, which is operated by the Association of Universities for Research in Astronomy, Inc., under NASA contract NAS 5-26555. These observations are associated with program 14223. This work is based on observations made with the NASA/ESA/CSA James Webb Space Telescope. The data were obtained from the Mikulski Archive for Space Telescopes at the Space Telescope Science Institute, which is operated by the Association of Universities for Research in Astronomy, Inc., under NASA contract NAS 5-03127 for *JWST*. These observations are associated with *JWST* program # 1176. *Software:* This research made use of astropy, a community developed core Python package for astronomy (Astropy Collaboration et al. 2018), APLpy, an open-source plotting package for Python (Robitaille & Bressert 2012), the IDL Astronomy Library (Landsman 1993); SIPGI (Gargiulo et al. 2022); Bagpipes (Carnall et al. 2021); EZ (Garilli et al. 2010); and CIGALE (Boquien et al. 2019).

References

- Aegeorges, N., Seifert, W., Jütte, M., et al. 2010, in Proc. SPIE, Vol. 7735, Ground-based and Airborne Instrumentation for Astronomy III, 77351L
- Aguirre, A. & Haiman, Z. 2000, *ApJ*, 532, 28
- Astropy Collaboration, Price-Whelan, A. M., Sipocz, B. M., et al. 2018, *AJ*, 156, 123
- Balogh, M. L., Morris, S. L., Yee, H. K. C., Carlberg, R. G., & Ellingson, E. 1999, *ApJ*, 527, 54
- Beichman, C. A., Rieke, M., Eisenstein, D., et al. 2012, in Society of Photo-Optical Instrumentation Engineers (SPIE) Conference Series, Vol. 8442, Space Telescopes and Instrumentation 2012: Optical, Infrared, and Millimeter Wave, ed. M. C. Clampin, G. G. Fazio, H. A. MacEwen, & J. Oschmann, Jacobus M., 84422N
- Belfiore, F., Maiolino, R., Maraston, C., et al. 2016, *MNRAS*, 461, 3111
- Bica, E., Alloin, D., & Schmitt, H. R. 1994, *A&A*, 283, 805
- Boquien, M., Burgarella, D., Roehly, Y., et al. 2019, *A&A*, 622, A103
- Bruzual, A. G. & Charlot, S. 2003, *MNRAS*, 344, 1000
- Buschkamp, P., Seifert, W., Polsterer, K., et al. 2012, in Proc. SPIE, Vol. 8446, Society of Photo-Optical Instrumentation Engineers (SPIE) Conference Series, 84465L
- Cañameras, R., Nesvadba, N. P. H., Limousin, M., et al. 2018, *A&A*, 620, A60
- Calzetti, D. 1997, *AJ*, 113, 162
- Calzetti, D., Armus, L., Bohlin, R. C., et al. 2000, *ApJ*, 533, 682
- Carnall, A. C., McLure, R. J., Dunlop, J. S., & Davé, R. 2021, Bagpipes: Bayesian Analysis of Galaxies for Physical Inference and Parameter Estimation, Astrophysics Source Code Library, record ascl:2104.017
- Chabrier, G. 2003, *PASP*, 115, 763
- Combes, F. 2004, *New A Rev.*, 48, 583
- D'Eugenio, C., Daddi, E., Gobat, R., et al. 2021, *A&A*, 653, A32
- Diego, J. M., Meena, A. K., Adams, N. J., et al. 2023, *A&A*, 672, A3
- Drell, P. S., Lored, T. J., & Wasserman, I. 2000, *ApJ*, 530, 593
- Farrah, D., Meikle, W. P. S., Clements, D., Rowan-Robinson, M., & Mattila, S. 2002, *MNRAS*, 336, L17
- Frye, B., Pascale, M., Cohen, S., et al. 2023, *Transient Name Server AstroNote*, 96, 1
- Frye, B. L., Pascale, M., Qin, Y., et al. 2019, *ApJ*, 871, 51
- Gardner, J. P., Mather, J. C., Clampin, M., et al. 2006, *Space Sci. Rev.*, 123, 485
- Gargiulo, A., Bolzonella, M., Scodreggio, M., et al. 2017, *A&A*, 606, A113
- Gargiulo, A., Fumana, M., Bisogni, S., et al. 2022, *MNRAS*, 514, 2902
- Garilli, B., Fumana, M., Franzetti, P., et al. 2010, *PASP*, 122, 827
- Haines, C. P., Iovino, A., Krywult, J., et al. 2017, *A&A*, 605, A4
- Hamuy, M., Phillips, M. M., Maza, J., et al. 1995, *AJ*, 109, 1
- Harrington, K. C., Yun, M. S., Cybulski, R., et al. 2016, *MNRAS*, 458, 4383
- Hill, J. M., Green, R. F., Ashby, D. S., et al. 2012, in Proc. SPIE, Vol. 8444, Ground-based and Airborne Telescopes IV, 84441A
- Höflich, P., Nomoto, K., Umeda, H., & Wheeler, J. C. 2000, *ApJ*, 528, 590
- Johnson, T. L. & Sharon, K. 2016, *ApJ*, 832, 82
- Jones, D. O., Rodney, S. A., Riess, A. G., et al. 2013, *ApJ*, 768, 166
- Kauffmann, G., Heckman, T. M., White, S. D. M., et al. 2003, *MNRAS*, 341, 33
- Kelly, P. L. & Kirshner, R. P. 2012, *ApJ*, 759, 107
- Kelly, P. L., Rodney, S., Treu, T., et al. 2023, *ApJ*, 948, 93
- Khetan, N., Cooke, J., & Branchesi, M. 2023, *MNRAS*, 521, 2814
- Landsman, W. B. 1993, in *Astronomical Society of the Pacific Conference Series*, Vol. 52, *Astronomical Data Analysis Software and Systems II*, ed. R. J. Hanisch, R. J. V. Brissenden, & J. Barnes, 246
- Meena, A. K., Zitrin, A., Jiménez-Teja, Y., et al. 2023, *ApJ*, 944, L6
- Miley, G. K., Overzier, R. A., Tsvetanov, Z. I., et al. 2004, *Nature*, 427, 47
- Oke, J. B. & Gunn, J. E. 1983, *ApJ*, 266, 713
- Pacifci, C., Iyer, K. G., Mobasher, B., et al. 2023, *ApJ*, 944, 141
- Pascale, M., Frye, B. L., Dai, L., et al. 2022, *ApJ*, 932, 85
- Planck Collaboration, Ade, P. A. R., Aghanim, N., et al. 2016, *A&A*, 596, A100
- Planck Collaboration, Aghanim, N., Akrami, Y., et al. 2020, *A&A*, 641, A6
- Planck Collaboration, Aghanim, N., Altieri, B., et al. 2015, *A&A*, 582, A30
- Rieke, M. J., Kelly, D., & Horner, S. 2005, in Society of Photo-Optical Instrumentation Engineers (SPIE) Conference Series, Vol. 5904, *Cryogenic Optical Systems and Instruments XI*, ed. J. B. Heaney & L. G. Burriesci, 1–8
- Robitaille, T. & Bressert, E. 2012, *APLpy: Astronomical Plotting Library in Python*
- Rodney, S. A., Riess, A. G., Scolnic, D. M., et al. 2015, *AJ*, 150, 156
- Rubin, D., Hayden, B., Huang, X., et al. 2018, *ApJ*, 866, 65
- Seifert, W., Aegeorges, N., Lehmitz, M., et al. 2010, in Proc. SPIE, Vol. 7735, Ground-based and Airborne Instrumentation for Astronomy III, 77357W
- Seifert, W., Appenzeller, I., Baumeister, H., et al. 2003, in Proc. SPIE, Vol. 4841, *Instrument Design and Performance for Optical/Infrared Ground-based Telescopes*, ed. M. Iye & A. F. M. Moorwood, 962–973
- Speagle, J. S., Steinhardt, C. L., Capak, P. L., & Silverman, J. D. 2014, *ApJS*, 214, 15
- Sullivan, M., Ellis, R. S., Aldering, G., et al. 2003, *MNRAS*, 340, 1057
- Sullivan, M., Le Borgne, D., Pritchett, C. J., et al. 2006, *ApJ*, 648, 868

- Totani, T. & Kobayashi, C. 1999, ApJ, 526, L65
- Vanzella, E., Claeysens, A., Welch, B., et al. 2023, ApJ, 945, 53
- Welch, B., Coe, D., Zackrisson, E., et al. 2022, ApJ, 940, L1
- Williams, B. F., Hogan, C. J., Barris, B., et al. 2003, AJ, 126, 2608
- Williams, S. C., Hook, I. M., Hayden, B., et al. 2020, MNRAS, 495, 3859
- Windhorst, R. A., Cohen, S. H., Jansen, R. A., et al. 2023, AJ, 165, 13
- Windhorst, R. A., Hathi, N. P., Cohen, S. H., et al. 2008, Advances in Space Research, 41, 1965
- Zhuang, M.-Y. & Ho, L. C. 2019, ApJ, 882, 89
- Zirm, A. W., Overzier, R. A., Miley, G. K., et al. 2005, ApJ, 630, 68
- ²⁷ Department of Physics and Astronomy, University of Missouri, Columbia, MO 65211, USA
- ²⁸ Department of Astronomy, University of Massachusetts at Amherst, Amherst, MA 01003, USA

-
- ¹ INAF – Istituto di Astrofisica Spaziale e Fisica Cosmica Milano, Via A. Corti 12, I-20133 Milano, Italy
- ² INAF-Osservatorio Astronomico di Trieste, Via Bazzoni 2, 34124 Trieste, Italy
- ³ Steward Observatory, University of Arizona, 933 N Cherry Ave, Tucson, AZ, 85721-0009, USA
- ⁴ Large Binocular Telescope Observatory, 933 North Cherry Ave, Tucson, AZ 85721, USA
- ⁵ Univ. Lyon, Univ. Lyon1, ENS de Lyon, CNRS, Centre de Recherche Astrophysique de Lyon UMR5574, F-69230 Saint-Genis-Laval, France
- ⁶ Department of Astronomy, University of California, 501 Campbell Hall #3411, Berkeley, CA 94720, USA
- ⁷ Center for Astrophysics | Harvard & Smithsonian, 60 Garden Street, Cambridge, MA 02138, USA
- ⁸ School of Earth and Space Exploration, Arizona State University, Tempe, AZ 85287-1404, USA
- ⁹ Chinese Academy of Sciences South America Center for Astronomy, National Astronomical Observatories, CAS, Beijing 100101, China
- ¹⁰ CAS Key Laboratory of Optical Astronomy, National Astronomical Observatories, Chinese Academy of Sciences, Beijing 100101, China
- ¹¹ Space Telescope Science Institute, 3700 San Martin Drive, Baltimore, MD 21218, USA
- ¹² Association of Universities for Research in Astronomy (AURA) for the European Space Agency (ESA), STScI, Baltimore, MD 21218, USA
- ¹³ Center for Astrophysical Sciences, Department of Physics and Astronomy, The Johns Hopkins University, 3400 N Charles St. Baltimore, MD 21218, USA
- ¹⁴ Jodrell Bank Centre for Astrophysics, Alan Turing Building, University of Manchester, Oxford Road, Manchester M13 9PL, UK
- ¹⁵ Department of Physics, University of California, 366 Physics North MC 7300, Berkeley, C. 94720, USA
- ¹⁶ FCA, Instituto de Física de Cantabria (UC-CSIC), Av. de Los Castros s/n, E-39005 Santander, Spain
- ¹⁷ Université Paris-Saclay, CNRS, Institut d’Astrophysique Spatiale, 91405, Orsay, France
- ¹⁸ International Centre for Radio Astronomy Research (ICRAR) and the International Space Centre (ISC), The University of Western Australia, M468, 35 Stirling Highway, Crawley
- ¹⁹ ARC Centre of Excellence for All Sky Astrophysics in 3 Dimensions (ASTRO 3D), Australia
- ²⁰ INAF Osservatorio Astronomico di Roma, Via Frascati 33, I-00078 Monteporzio Catone, Rome, Italy
- ²¹ Physics Department, Ben-Gurion University of the Negev, P. O. Box 653, Be’er-Sheva, 8410501, Israel
- ²² European Southern Observatory, Alonso de Córdova 3107, Vitacura, Casilla 19001, Santiago de Chile, Chile
- ²³ School of Physics and Astronomy, University of Minnesota, 116 Church Street SE, Minneapolis, MN 55455, USA
- ²⁴ National Research Council of Canada, Herzberg Astronomy & Astrophysics Research Centre, 5071 West Saanich Road, Victoria, BC V9E 2E7, Canada
- ²⁵ Minnesota State University-Mankato, Telescope Science Institute, TN141, Mankato MN 56001, USA
- ²⁶ Max-Planck-Institut für extraterrestrische Physi, Garching, 85741, Germany